Charge−Discharge Properties of Sputtered Mg Anode in Flexible All-Solid-State Mg-Ion Batteries

Kuan-Jen Chen,* Fei-Yi Hung,* and Yen-Ting He

Read Online

ACCESS | Metrics & More | Article Recommendations

ABSTRACT: In this study, a sputtered Mg film was fabricated as an anode, a natural magnesium silicate mineral was used as electrolyte, and an all-solid-state Mg battery with a carbon black electrode was assembled; subsequently, the battery's electrochemical characteristics and charge−discharge mechanism were evaluated. Because the abundant interlayer water in the magnesium silicate mineral structure allowed for cations channel to form, the battery exhibited considerable ionic conductivity at room temperature. The magnesium silicate mineral was fabricated as a flexible cloth membrane solid-state electrolyte to improve its adhesion to the electrode surface and, consequently, enhance battery performance. During high-voltage charging, a visible blocking layer structure was formed on the surface of the Mg electrode. The formation of the blocking layer considerably increased the interfacial resistance of the battery, which was detrimental to the insertion and extraction of the Mg ions on the electrode surface and reduced the capacity of the solid-state battery. Thus, the solid-state Mg battery exhibited acceptable capacity and stability and the potential for application in energy storage systems.
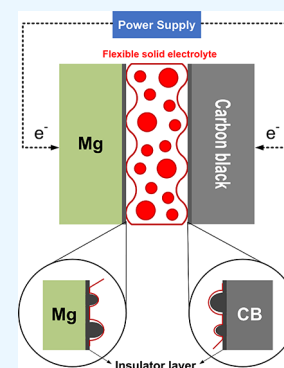
1. INTRODUCTION

Because of the trend pertaining to net zero CO_2 emissions, renewable energy and electric vehicles are becoming key components of the green energy policies of various countries.[1,2] Therefore, secondary ion batteries with high levels of performance and safety must be developed. To this end, research studies are increasingly exploring the use of non-Li-ion secondary,[3−7] among which Mg-ion batteries exhibit considerable potential for application in energy storage systems.[8] Mg has a considerable theoretical capacity (3833 mAh/cm^3), and Mg mineral reserves are larger than those of Li; thus, the sue of Mg in place of Li can reduce the cost of anode materials.[9] In addition, dendritic structures do not form and accumulate on a Mg electrode surface, and this property of Mg electrode eliminates the risk of explosions caused by battery short circuits. At the time of writing, two primary types of electrodes are prepared, namely, powder-based electrodes and thin-film electrodes.[10,11] Powder-based electrodes are fabricated by mixing active materials with an adhesive and then applying the mixture as a coating on the collector-layer material (Cu or Al foil). However, the active material density of an electrode obtained through the coating method is low, and the bonding characteristics between a Cu foil and active material must be considered. Furthermore, Mg exhibits considerable activity, such that Mg powder is easily oxidized by physical grinding. Thus, in this study, a Mg-film anode is fabricated by depositing pure Mg on a Cu foil through radio frequency sputtering. A high-quality Mg-film electrode can be obtained through sputtering, and the formation of an

intermetallic compound (IMC) can enhance the bonding between a Cu matrix and active materials.[12,13]

The electrolytes of commercial Li batteries are mostly toxic organic solvents (e.g., $LiPF_6$, $LiAsF_6$ $LiBF_6$, $LiClO_4$),[14,15] which have low burning points and low thermal stability; consequently, these solvents increase the risk of batteries exploding due to inappropriate operation or impact. To solve the aforementioned problem of organic liquid electrolytes, researchers have developed Li-ion solid polymer electrolytes[16] and Li-ion inorganic solid electrolytes.[17] A solid polymer electrolyte exhibits a colloid-like state, which benefits ion transportation, inhibits the formation of dendrites, and increases impact resistance such that battery safety is improved.[18] Inorganic solid electrolytes (also known as ionic superconductors) exhibit high ionic conductivity at room temperature. Numerous studies have proposed the use of lithium oxides as solid electrolytes (e.g., perovskite, NASICON, LISICON, and LiPON systems),[19−21] which exhibit acceptable ionic conductivity and low activation energy at room temperature. However, the use of Li-based solid electrolytes is limited by the scarcity of Li mineral reserves.

On the basis of the aforementioned findings, the present study used an inorganic solid electrolyte with stable chemical

properties, a wide operating temperature range, and an applicable electrochemical window. In addition, it can perform the function of a conventional battery's separators. The conduction mechanism of solid-state ions operates through the lattice defects of electrolyte materials, which serve as ion transfer channels. Therefore, the concentration of internal defects affects the ionic conductivity of solid electrolytes. In the present study, natural magnesium silicate mineral was used as the solid electrolyte material of a battery. The abundance of water molecules in the layered crystals of magnesium silicate minerals can promote ion conduction, which improves the performance of the solid electrolyte at room temperature.[5] Furthermore, magnesium silicate minerals combine with polymer to form a flexible electrolyte membrane, which promotes adhesion to an electrode surface and enhances charge–discharge performance.

The present study used a sputtered Mg-film anode, a flexible Mg silicate electrolyte, and a carbon black (CB) cathode to assemble all-solid-state Mg batteries. The produced batteries were subjected to various charge–discharge rates (0.1, 0.2, and 0.5 mA) and operating temperatures (25 and 55 °C) to evaluate their cycle performance. In addition, the surface characteristics of the Mg anode and electrolytes after an electrochemical cycle reaction were examined to clarify the failure mechanism of the batteries.

2. EXPERIMENTAL PROCEDURE

The present study used a sputtered Mg film (thickness of approximately 400 nm) as anode material, and it evaluated the effects of electrolyte materials on the charge–discharge characteristics of the assembled batteries. Sputtered Mg films (anode), CB electrode (cathode), and lithium hexafluorophosphate ($LiPF_6$) electrolytes were incorporated into wet half-cells, which were then tested for charge–discharge performance.

Subsequently, the sputtered Mg anode was used to fabricate of all-solid-state batteries. The CB (90 wt %) and polyvinylidene fluoride (10 wt %) were mixed with an N-methylpyrrolidone solvent and then coated on Al foils (thickness of approximately 15 μm) to serve as counter electrodes (cathode). The CB electrodes were baked in an oven at 55 °C for 12 h and then cut into disks (diameter of 13 mm in diameter and thickness of approximately 200 μm). Magnesium silicate mineral powder was used to fabricate ingot and flexible cloth membrane (FCM) solid-state electrolytes (Figure 1a). The ingot electrolyte (diameter of 13.5 mm and thickness of approximately 600 μm) was obtained by performing cold isostatic pressing at a pressure of 60 kg/cm^2 for 1 min. In addition, the magnesium silicate mineral powder and polymer were mixed with a weight ratio of 1:19 at 170 °C and then hot-pressed at a pressure of 50 kg/cm^2 to form the FCM solid-state electrolyte (thickness of approximately 250 μm). Subsequently, the sputtered Mg anode, the solid-state electrolyte membrane, and the CB cathode were used to assemble an all-solid-state battery (Mg/solid-state electrolytes/CB) (Figure 1b).

The surface characteristics and phase composition of the electrodes were analyzed using a high-resolution scanning electron microscope (HITACHI/SU8000) and a multipurpose X-ray thin-film micro-area diffractometer (XRD, Bruker D8 Discover) with Cu Kα radiation, respectively. Impedance analysis of the solid-state electrolytes was conducted using an electrochemical impedance spectroscope (EIS, PARSTAT
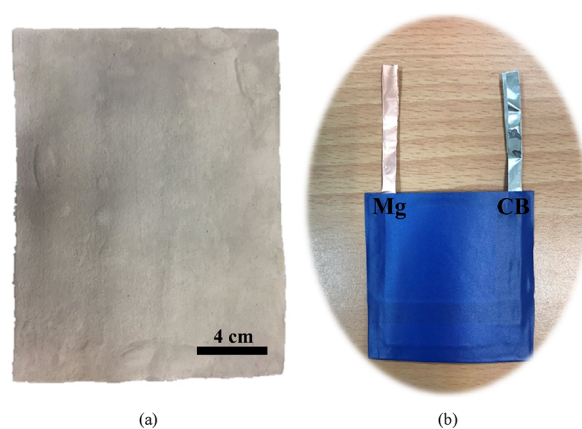

(a)   (b)

Figure 1. Macrograph images of (a) FCM and (b) flexible full battery.

2273); the analysis was performed by applying an AC voltage at an amplitude of 10 mV amplitude and a frequency range of 0.1 Hz to 100 kHz. After charge–discharge cycle testing was performed, the phase composition of the solid-state electrolytes was analyzed through Fourier-transform infrared spectrometry (FTIR) performed in transmission mode at a frequency range of 500–4000 cm^{-1} and resolution of 1 cm^{-1}/s. Electrochemical cycle testing was performed using a battery testing cell and a battery automatic tester (BAT-750B). The assembled wet-cell and solid-state batteries were tested at various charge–discharge rates. In addition, the effects of a high operating temperature (55 °C) on the charge–discharge performance of the assembled batteries were investigated.

3. RESULTS AND DISCUSSION

3.1. Performance of Wet-Cell Mg Battery. The surface morphology of a pure Mg-film electrode as obtained after sputtering deposition is displayed in Figure 2a, which reveals that numerous hexagonal grains had formed on the Cu foil after sputtering. The sputtered Mg-film electrodes exhibited a comparable flatness, which promotes contact reactions between the electrode and electrolyte. Figure 2b displays the XRD pattern of the sputtered Mg electrode, which mainly comprised Cu and Mg phases. The presence of Cu phases was attributed to the Cu foil matrix. The signal of the sputtered Mg film preferred an orientation of (002), which indicated that the Mg had a hexagonal close-packed crystal structure.

Charge–discharge cycle testing was conducted to estimate the effects of various charge–discharge rates on the cycling performance of the wet-cell batteries (Mg/$LiPF_6$/CB). At the charge–discharge rate of 0.1 mA (Figure 3a), the battery capacity of the wet-cell batteries peaked during the first cycle. Subsequently, their capacity gradually decreased with an increase in cycle number and finally stabilized after 50 cycles. This result indicates that electrolyte ions reacted with the electrode surface of the batteries to form a solid-electrolyte interface layer during the initial charge–discharge reaction.[22] This irreversible reaction provided a long insertion time for ions, thereby enhancing the performance of the initial charge–discharge. The subsequent charge–discharge cycles belonged to the reversible reaction of insertion and extraction for ions, which increased the stability of the cycling performance of the batteries. With an increase in the C rate (Figure 3b,c), a considerable capacity was also attained in the first cycle, but it rapidly decreased and then gradually decreased and stabilized when the cycle number was increased. In addition, excluding
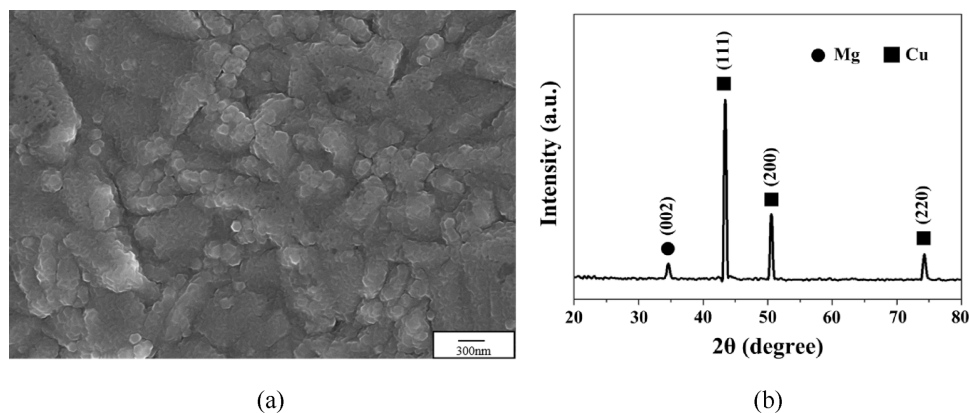
(a)

(b)

Figure 2. (a) Surface morphology and (b) X-ray thin-film micro-area diffractometry pattern of the sputtered Mg-film electrode.
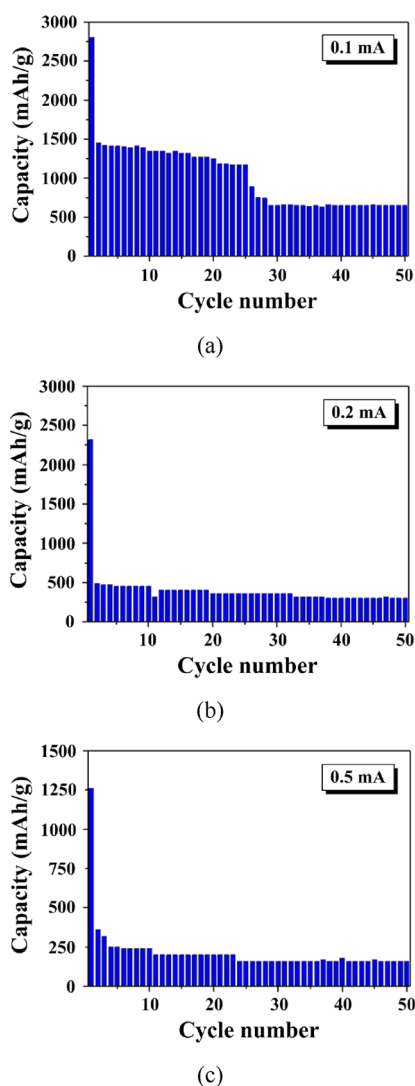

(a)

(b)

(c)

Figure 3. Cycle performance of the wet-cell Mg-ion battery at various charge−discharge rates: (a) 0.1, (b) 0.2, and (c) 0.5 mA.

the initial charge−discharge capacity, the average capacity of the batteries was 1052 mAh/g at the 1C charge−discharge rate; however, their degradation rate, i.e.,

$$\text{decay rate (\%)} = \frac{\text{the 2nd cycle capacity} - \text{capacity in the last cycle}}{\text{the 2nd cycle capacity}} 100$$

for the battery performance was approximately 57%. Furthermore, the average capacity of the batteries decreased to 325 and 190 mAh/g when the charge−discharge rate increased to 0.2 and 0.5 mA, respectively, and their battery performance also exhibited a considerable decline rate.

The aforementioned results indicate that the difference between the charge transfer rate and the lithiation/delithiation reaction rate of the batteries was small when their charge−discharge rate was low. Li ions had sufficient time to react with the lithiation and delithiation sites between electrodes; thus, the lithiation reaction on the electrode surface was enhanced. However, a long duration charge−discharge cycling duration resulted in a considerable deterioration rate. At a high charge−discharge rate, a rapid charge transfer affected the lithiation of the ions on the electrode surface and caused electrochemical reactions to concentrate on the electrode surface. Although a high charge−discharge rate reduced the deterioration rate in the electrode, the batteries' capacity was low because of the occurrence of localized electrochemical reactions. After numerous charge−discharge cycles, the reduction of the localized electrochemical reaction area was greater in the battery with a high C rate than in the battery with a low C rate; thus, the decay rate for battery cycle life was still considerable.

The wet-cell battery materials that were assembled in a cylindrical 18,650 battery cell for charge−discharge cycle testing is displayed in Figure 4. Before electrochemical cycle testing was conducted, the assembled 18,650 battery was activated by applying a 10 mA current. Next, the battery was conducted at a charge−discharge rate of 1 mA, and the cut-off voltage was set to 10−2500 mV. The wet-cell 18,650 battery exhibited stable charge−discharge characteristics and did not degrade notably during the 50 cycle test. This result indicates
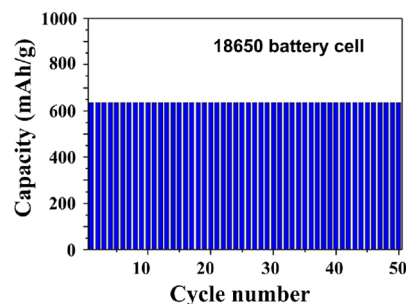

Figure 4. Charge−discharge cycle performance of the wet-cell 18,650 battery.
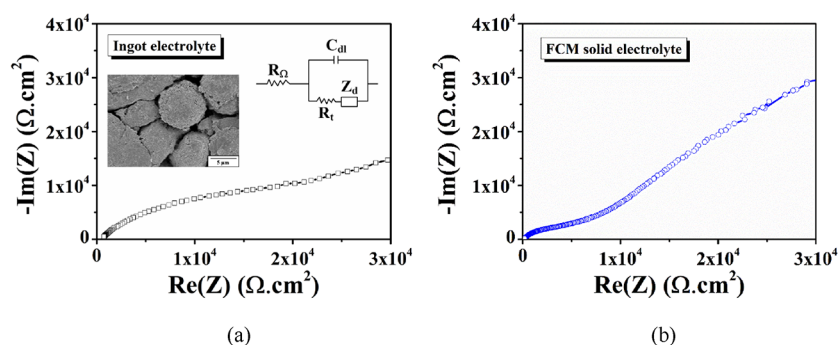
Figure 5. Electrochemical impedance analysis of (a) ingot and (b) FCM solid electrolytes.

that the large volume of the 18,650 battery can increase the contact area between its electrodes and electrolyte, which increases its effective electrochemical reaction area.

3.2. Performance of Solid-State Mg Battery. The sputtered Mg film, which was used as anode materials, exhibited favorable performance for ion batteries. Therefore, the sputtered Mg-film electrodes were combined with various types of solid-state electrolytes in all-solid-state batteries to evaluate the ionic conductivity of various electrolytes. The ionic conductivity of an electrolyte material must be $>10^{-4}$ S/cm to ensure that it has sufficient ion transport capacity. Through EIS measurements, the impedance spectra of the solid-state battery, as visualized on the Nyquist plane, are presented in Figure 5. The intersection between the high-frequency region and the X-axis is the electrolyte impedance (R_Ω), which indicates the impedance of ion conduction in the electrolyte. In addition to an electrolyte's resistance, an electrode's SEI layer, a separator, and an electrode material also affect electrolyte impedance (R_Ω). Electrostatic double-layer capacitor (C_{dl}) exists between the electrode and the electrolyte in the electrochemical reaction. When ions were inserted into an electrode, the ions and the electrode underwent a redox reaction, which involved the transfer of oxidative charges. The resistance that the charge transfer needs to overcome is the charge transfer resistance (R_t). In addition, Warburg diffusion (Z_d) is expressed as the impedance formed by the diffusion of ions in the electrolyte, also known as the Warburg impedance. Based on the above results, the resulting electrolyte impedance can be converted to ionic conductivity, and its formula is as follows:

$$\sigma = \frac{l}{R_\Omega A}$$

where σ is the ionic conductivity, l is the length (electrolyte thickness), R_Ω is the electrolyte impedance, and A is the contact area between the electrolyte and electrode.

The ionic conductivity levels of 1.78×10^{-4} and 4.86×10^{-3} S/cm correspond to the ingot electrolyte and FCM electrolytes, respectively. This result indicates that the ionic conductivity of both electrolytes meets the application requirement for solid-state batteries. Notably, relative to the ingot electrolyte, the FCM electrolyte exhibited greater adhesion to the electrode surface and, consequently, a higher ionic conductivity.

The solid-state batteries were conducted at a charge–discharge rate of 0.01 mA for 1080 min, and the cut-off voltage was set to 10−1900 mV. Figure 6a presents the charge–discharge cycle test results for the Mg-ion solid-state battery
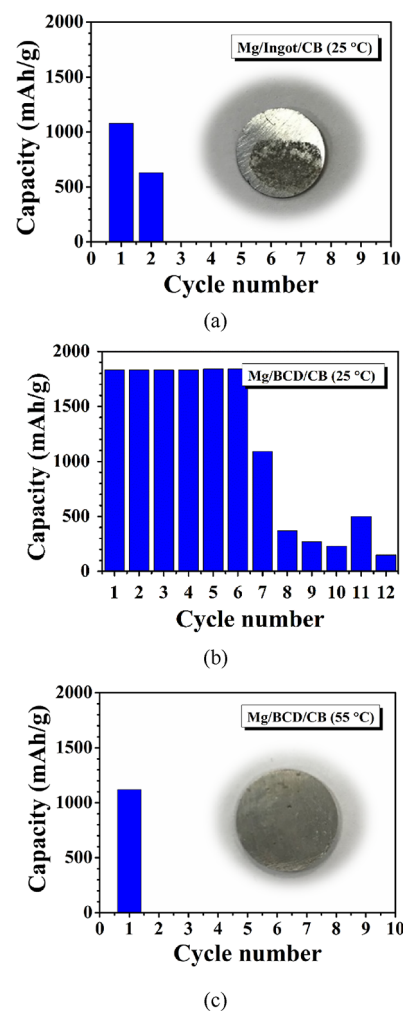

Figure 6. Cycle performances of solid-state Mg batteries: (a) Mg/Ingot/C at 25 °C, (b) Mg/FCM/C at 25 °C, and (c) Mg/FCM/C at 55 °C (abbreviation: FCM, flexible cloth membrane).

that was assembled with an ingot electrolyte. The capacity of this battery peaked (1080 mAhg^{-1}) during the initial cycle and then decreased to failure within 2 cycles. The charge–discharge cycle test results reveal the presence of an erosion layer with the same color as that of the electrolyte on the Mg electrode surface. This result indicates that this erosion layer retarded the contact between the electrode and electrolyte surface, thereby reducing the capacity of the battery. In addition, relative to the FCM electrolyte, the ingot electrolyte

exhibited less uniform adhesion to the electrode surface and, consequently, a smaller electrochemical reaction area.

The electrolyte material in the solid-state Mg battery was replaced with the FCM electrolyte, and the battery was conducted to perform charge—discharge cycle testing (Figure 6 b). The battery's capacity peaked at 1830 mAhg^{-1}, and it maintained a stable charge—discharge cycle performance for six cycles; subsequently, its capacity decreased substantially until the seventh cycle. The Mg/FCM/C battery exhibited acceptable charge—discharge cycle stability relative to the Mg/Ingot/C battery. The FCM electrolyte was flexible, which promoted its adhesion to the electrode surface and increased the size of the electrochemical reaction area. At a high operating temperature (55 °C), the battery's maximum discharge capacity decreased to 1120 mAhg^{-1}, and only one cycle life remained (Figure 6c). This result indicates that the operating temperature substantially influenced the battery performance.

Table 1 shows the EDS results of the ingot electrolyte surface before and after charge—discharge testing. Magnesium

Table 1. Energy Dispersive X-Ray Spectroscopy Analysis of Ingot Electrolyte Surface before and after Charging and Discharging

	at. %				
element	Na	Mg	Al	Si	O
before charge—discharge	1.76	2.09	13.43	48.33	34.40
after charge—discharge	0.89	6.81	12.39	47.58	32.33

silicate mineral is mainly composed of aluminum oxide and silicon oxide, and its surface composition is mainly composed of Si, Al, and O elements. The atomic concentration of Ma and Na in the as-fabricated ingot electrolyte was similar. After charge—discharge testing, the atomic ratio of Mg increased, but that of Na decreased from 1.76 to 0.89 at. %. These results indicate that Mg and Na ions served as cation carriers during the charge—discharge process.

To clarify the effects of electrochemical reactions on battery cycle performance, the state of the electrolytes before and after charge—discharge testing was subjected to an XRD analysis (Figure 7). The ingot electrolyte (magnesium silicate mineral)
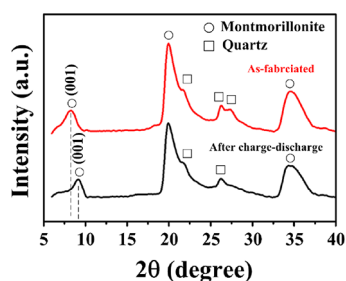
Figure 7. X-ray thin-film micro-area diffractometry patterns of magnesium silicate mineral electrodes obtained before and after charge—discharge cycle testing.

mainly comprised montmorillonite and quartz phases. The ingot electrolyte retained its diffraction peak after it underwent charge—discharge cycle testing at room temperature, indicating that it maintained a stable crystal structure. The intensity of its diffraction peaks decreased considerably after charge—discharge cycling, indicating the disintegration of its montmorillonite structure. Furthermore, the (001) diffraction peak

of the electrolyte shifted to a high angle after charge—discharge cycling. The montmorillonite structure in a magnesium silicate mineral is arranged in layered (001) crystal planes that contains considerable amounts of interlayer water and cations, which can as a conduction channel and a source of ions. On the basis of Bragg's law ($\lambda = 2d\sin\theta$),[23] the interlayer distance between the (001) planes was determined to have decreased from 11.75 to 9.59 Å. This result indicates that the water molecules or cations in the interlayer were consumed, resulting in a decrease in the interlayer distance between the (001) planes.

In addition, to understand the transport mechanism of electrolyte materials, the electrolytes were examined through an FTIR analysis after they were subjected to charge—discharge cycling at various temperatures (Figure 8).
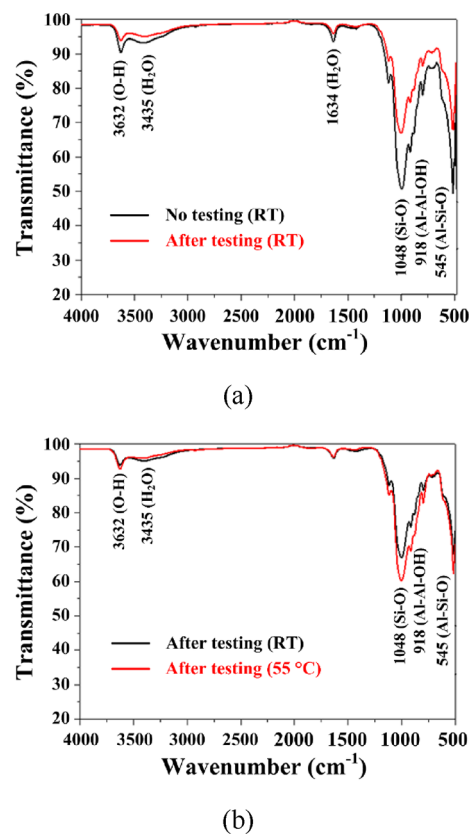
(a)

(b)

Figure 8. Fourier-transform infrared spectrometry analysis of solid-state electrodes obtained before and after charge—discharge cycle testing at various operating temperatures: (a) room temperature (RT) and (b) RT and 55 °C.

Magnesium silicate mineral is composed of silicates and aluminum oxide salts, and it contains the signals of water molecule and hydroxide bonding (Figure 8a). The overall bonding signal of the solid electrolyte decreased after charge—discharge cycling. In particular, the signals of Si—O and Al—Si—O bonds decrease substantially, indicating the disintegration of montmorillonite structures during the charge—discharge cycle. Furthermore, the signal of water molecules decreased, indicating the termination of the electrochemical reaction that is associated with a decrease in the amount of interlayer water. A comparison of the solid electrolytes' FTIR analysis results as obtained after charge—discharge cycling at various temperatures was performed, and the results are

presented in Figure 8b. Notably, both batteries could not proceed with the electrochemical reaction. The signal of their silicate structure at 55 °C was stronger than that at room temperature; however, the signal of their water molecules was weaker at high temperatures than at low temperatures. In brief, the termination of electrochemical reactions was related to the disintegration of layered structures. The decrease in the amount of interlayer water molecules was the main factor that affected the battery charge–discharge performance.

To clarify the effects of charge–discharge rates on battery performance, the solid-state battery was tested at various current rates with a cut-off time of 1080 min (Figure 9). At a
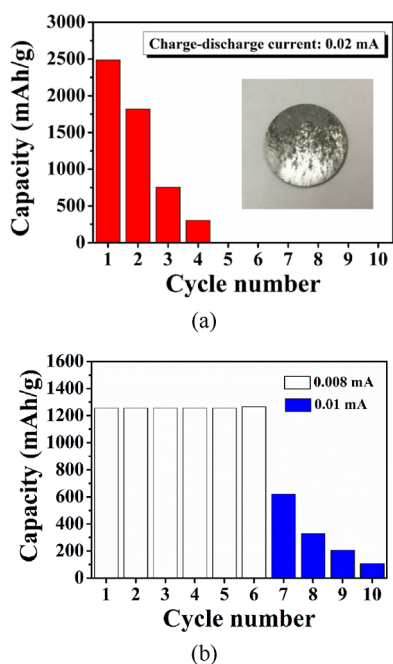

(a)

(b)

Figure 9. Cycle performance of the solid-state Mg battery at different charge–discharge rates: (a) 0.02 and (b) 0.008 and 0.01 mA.

high charge–discharge rate (0.02 mA), the battery's capacity peaked at 2490 mAh/g during the initial cycle and decreased considerably in the subsequent cycles (Figure 9a). The high current rate of 0.02 mA promoted the battery's capacity during the first cycle but caused it to rapidly decrease to failure within four cycles. The decrease in the battery's cycle life was due to the rapid insertion and extraction of ions, which resulted in the accumulation of ions on the electrode surface and reduced the battery's capacity.[24] At a low charge–discharge rate (0.008 mA), the battery's maximum capacity decreased to 1260 mAh/g; however, its cycle life was similar to that of the battery that was subjected to a charge–discharge rate of 0.01 mA (Figure 9b). Notably, the battery maintained a stable charge–discharge capacity for six cycles and then failed immediately in the subsequent cycle. To clarify the battery's performance after the sixth cycle, the charge–discharge cycle test was repeated for the failed battery at a high charge–discharge rate (0.01 mA). The failed battery produced an electrochemical reaction; however, its capacity decreased by 50% in this cycle and subsequently decreased to failure within four cycles. This result indicates that increasing the charge–discharge current enabled it to penetrate the thinner area of the erosion layer (blocking layer), providing the ions with sufficient kinetic energy to move to the electrode surface to cause an electrochemical reaction.

To clarify the effect of the blocking layer (formed on the electrode surface) on the cycle stability of the solid-state Mg battery, the composition of the blocking layer was examined through an energy dispersive X-ray spectroscopy (EDS) analysis. The solid-state battery was conducted under extreme charging conditions to form a thick blocking layer on the Mg electrode for analysis. The solid-state battery was charged at a constant voltage of 6 V for 1080 min and discharged at a constant current of 0.01 mA for 1080 min, and the cut-off voltage was set to 10–5000 mV. Under these conditions, the capacity (1220 mAh/h) of the battery peaked in the first cycle and subsequently decreased to failure within five cycles (Figure 10a). The battery's performance in this test was considerably
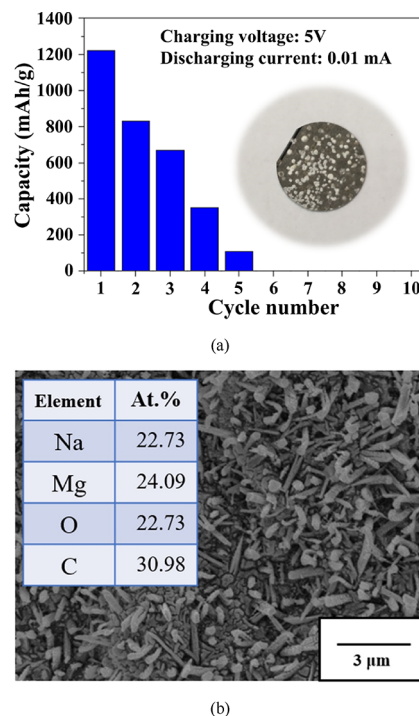

(a)

(b)

Figure 10. (a) Cycle performances of solid-state Mg batteries obtained after application of a charging voltage of 5 V and a discharging current of 0.01 mA. (b) Surface morphology of the Mg electrode obtained after high-voltage charging.

poorer relative to its performance in the charge–discharge test that was performed with a constant current of 0.01 mA (Figure 6b). This result indicates that the cations rapidly reacted with the electrode surface to form a blocking layer during the initial charge–discharge reaction, which considerably reduced the battery's performance. A macrograph image of the Mg electrode reveals the presence of white point-like accumulations that were distributed across the electrode surface. The surface morphology of the electrode indicates that these accumulations comprised numerous particle structures and needle-like crystals (Figure 10b). The results from the EDS analysis reveal that the accumulations mainly comprised the elements Na, Mg, C, and O. In addition, a considerable amount of C was detected, which came from the C on the long molecular chain of the polymer film. High-voltage charging damaged these long carbon chain structures, causing some carbon ions to react with the Mg electrode through the solid-state electrolyte.
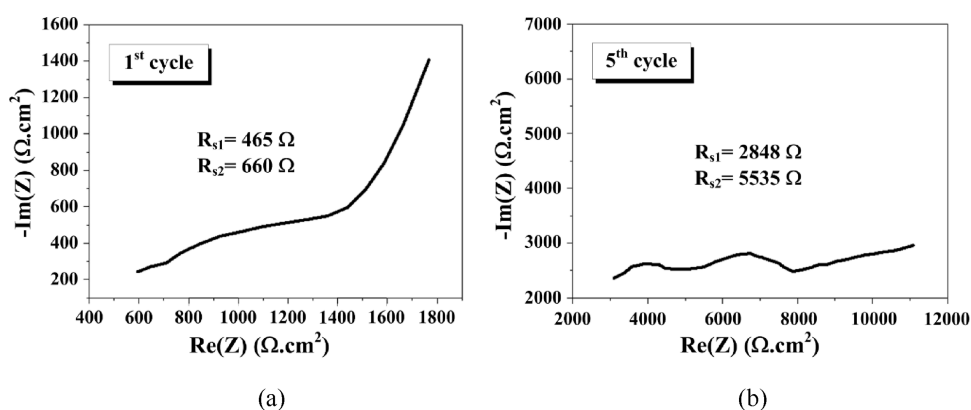
Figure 11. Electrochemical impedance analysis obtained after high-voltage charging: (a) first cycle, and (b) fifth cycle. Abbreviations: resistance, R_{s1}; surface resistance, R_{s2}.

Figure 11 presents the impedance spectra of the solid-state Mg battery as obtained after high-voltage charging at 5 V. The figure reveals that an extra small semicircle appeared in the high frequency region after the first round of high-voltage charging (Figure 11a). This result indicates that an additional interface layer was formed between the electrode and the FCM electrolyte and that it affected the transport of ions to the electrode surface. The semicircle in the medium frequency region was due to the interfacial resistance between the interface layer and the electrode surface. The resistance (R_{s1}) and the surface resistance (R_{s2}) of the interface layer and the electrolyte were still small during the first cycle, and their effects on the transport of ions in the battery were within the acceptable range. After five high-voltage charging cycles (Figure 11b), the resistance between the interface layer and the electrolyte increased considerably, and the interfacial resistance of the electrode surface increased considerably. This result indicates the reduced insertion and extraction of ions, which reduced the battery's performance. On the basis of the aforementioned results, the sputtered Mg film is a suitable anode material for all-solid-state batteries; however, its electrochemical characteristics under rapid charging conditions must be improved.

4. CONCLUSIONS

A sputtered Mg film was fabricated for use as an anode material, and it was combined with an FCM electrolyte and a CB cathode to assemble an all-solid-state battery. The sputtered Mg electrode exhibits considerable compactness, which can reduce electrode deterioration after charge–discharge cycling. Furthermore, the considerable flatness of the electrode's surface increases its contact area with the solid electrolyte of a solid-state battery.

The layered (001) crystal planes of montmorillonite structure in a magnesium silicate mineral are suitable as a transport channel for cations. The FTIR results reveal that a considerable amount of metal cations in the interlayer water of the electrolyte structure can serve as a transmission medium. The FCM magnesium silicate mineral electrolyte exhibits an acceptable ionic conductivity (4.86×10^{-3} S/cm) at room temperature different from the traditional solid electrolyte that use defect transitions. Furthermore, the solid-state battery with the FCM electrolyte achieved an acceptable level of charge–discharge cycle performance because of the favorable adhesion

between the FCM electrolyte and the electrode, which allowed for a favorable charge–discharge capacity to be achieved.

A prominent blocking layer formed after the high-voltage charge–discharge cycle test was conducted. This blocking layer comprised the elements Na, Mg, O, and C, which retarded the insertion and extraction of ions between the electrode and electrolyte and reduced cycling stability. Therefore, improving the interfacial adhesion in the structure of the solid-state battery can improve its charge–discharge cycle performance.

■ AUTHOR INFORMATION

Corresponding Authors

Kuan-Jen Chen − *Department of Mechanical Engineering, Southern Taiwan University of Science and Technology, Tainan 710, Taiwan;* orcid.org/0000-0002-9624-221X; Phone: 886-6-2533131-3921; Email: kjchen@stust.edu.tw

Fei-Yi Hung − *Department of Materials Science and Engineering, National Cheng Kung University, Tainan 701, Taiwan;* Phone: 886-6-2757575-62950; Email: fyhung@mail.ncku.edu.tw; Fax: 886-6-2346290

Author

Yen-Ting He − *Department of Materials Science and Engineering, National Cheng Kung University, Tainan 701, Taiwan*

Complete contact information is available at:
https://pubs.acs.org/10.1021/acsomega.2c05843

Notes

The authors declare no competing financial interest.

■ REFERENCES

(1) Hwang, I. S.; Lee, Y. H.; Ganesan, V.; Hwa, Y.; Park, C. M. High-energy-density gallium antimonide compound anode and optimized nanocomposite fabrication route for Li-ion batteries. *ACS Appl. Energy Mater.* **2022**, *5*, 8940−8951.

(2) Heath, G. A.; Ravikumar, D.; Hansen, B.; Kupets, E. A critical review of the circular economy for lithium-ion batteries and photovoltaic modules- status, challenges, and opportunities. *J. Air Waste Manag. Assoc.* **2022**, *72*, 478−539.

(3) Liu, Y.; Sun, Z.; Tan, K.; Denis, D. K.; Sun, J.; Liang, L.; Hou, L.; Yuan, C. Recent progress in flexible non-lithium based rechargeable batteries. *J. Mater. Chem. A* **2019**, *7*, 4353−4382.

(4) Benti, N. E.; Gurmesa, G. S.; Geffe, C. A.; Mohammed, A. M.; Tiruye, G. A.; Mekonnen, Y. S. Sodium-ion diffusion studies of the cathode-electrolyte interfaces (NaxO2@Na2CO3, x= 1 and 2) and discharge products of non-aqueous rechargeable sodium-air batteries. *J. Mater. Chem. A* **2022**, *10*, 8501−8514.

(5) Chen, K. J. Rechargeable all-solid-state tin ion battery in a low-temperature environment. *Results Mater.* **2021**, *10*, No. 100190.

(6) Zhao, R.; Wang, H.; Du, H.; Tang, Y.; Gao, Z.; Qie, L.; Huang, Y. Lanthanum nitrate as aqueous electrolyte additive for favourable zinc metal electrodeposition. *Nat. Commun.* **2022**, *13*, 3252.

(7) Zhu, G.; Wang, W.; Yu, X. Benzoate anion derived carbon-encapsulated NiS nanoparticles as a freestanding cathode for magnesium-based batteries. *J. Alloy. Comp.* **2022**, *919*, No. 165835.

(8) Hwang, Y. Y.; Lee, N. K.; Park, S. H.; Shin, J.; Lee, Y. J. TFSI anion grafted polymer as an ion-conducting protective layer on magnesium metal for rechargeable magnesium batteries. *Energy Storage Mater.* **2022**, *51*, 108−121.

(9) Zhou, Z.; Du, A.; Kong, W.; Chen, Z.; Zhang, Z.; Chen, B.; He, Y.; Dong, S.; Li, Z.; Li, G.; Cui, G. High area-capacity Mg batteries enabled by sulfur/copper integrated cathode design. *J. Energy Chem.* **2022**, *72*, 370−378.

(10) Zhou, Y.; Roginskii, E. M.; Smirnov, K. S.; Smirnov, M. B.; Savin, A. V.; Nguyen, O.; Pereira-Ramos, J. P.; Baddour-Hadjean, R. Insights into the electronic structure and vibrational dynamics of Li7MnN4 anode material for Li-ion battery: A combined experimental and computational study. *J. Alloy. Compd.* **2022**, *921*, No. 166004.

(11) Qi, L.; Lu, Z.; Liu, L.; Lu, P.; Sun, H.; Zhang, H. Annealing temperatures dependence of features of Sn-Ni-Cu alloy film as anode for lithium-ion batteries. *Chem. Phys. Lett.* **2022**, *800*, No. 139685.

(12) Bhasin, V.; Nayak, C.; Biswas, A.; Halankar, K. K.; Tokas, R. B.; Ghosh, S. K.; Bahadur, J.; Bhattacharyya, D. Remarkably high capacity Li ion batteries with rf sputter deposited TiO$_2$ thin film anodes on SS substrates. *Appl. Surf. Sci.* **2022**, *592*, No. 153273.

(13) Lee, J. H.; Cho, Y. G.; Gu, D.; Kim, S. J. 2D PdTe$_2$ thin-film-coated current collectors for long-cycling anode-free rechargeable batteries. *ACS Appl. Mater. Interfaces* **2022**, *14*, 15080−15089.

(14) Rodriguez, J. R.; Belman-Rodriguez, C.; Aguirre, S. B.; Aguila, S. A.; Pol, V. G. Influence of the fluoroethylene carbonate on the electrochemical behavior of Bi$_3$Ge$_4$O$_{12}$ as lithium-ion anode. *J. Colloid Interface Sci.* **2022**, *627*, 64−71.

(15) Kasse, R. M.; Geise, N. R.; Sebti, E.; Lim, K.; Takacs, C. J.; Cao, C.; Steinruck, H. G.; Toney, M. F. Combined effects of uniform applied pressure and electrolyte additives in lithium-metal batteries. *ACS Appl. Energy Mater.* **2022**, *5*, 8273−8281.

(16) Tian, L. W.; Kim, J. W.; Hong, S. B.; Ryu, H. H.; Kim, U. H.; Sun, Y. K.; Kim, D. W. All-solid-state lithium batteries featuring hybrid electrolytes based on Li$^+$ ion-conductive Li7La3Zr2O12 framework and full-concentration gradient Ni-rich NCM cathode. *Chem. Eng. J.* **2022**, *450*, No. 138043.

(17) Zhang, X.; Sun, Y.; Ma, C.; Guo, N.; Fan, H.; Liu, J.; Xie, H. Li6.4La3Zr1.4Ta0.6O12 reinforced polystyrene-poly (ethylene oxide)-poly (propylene oxide)-poly (ethylene oxide)-polystyrene pentablock copolymer-based composite solid electrolytes for solid-state lithium metal batteries. *J. Power Sources* **2022**, *542*, No. 231797.

(18) Yuan, B.; Cong, Z.; Cheng, Z.; Li, L.; Xia, L.; Yan, J.; Shen, F.; Zhao, B.; Han, X. Bacteria cellulose framework-supported solid composite polymer electrolytes for ambient-temperature lithium metal batteries. *Nanotechnology* **2022**, *33*, 415401.

(19) Pan, L.; Sun, S.; Yu, G.; Liu, X. X.; Feng, S.; Zhang, W.; Turgunov, M.; Wang, Y.; Sun, Z. Stabilizing solid electrolyte/Li interface via polymer-in-salt artificial protection layer for high-rate and stable lithium metal batteries. *Chem. Eng. J.* **2022**, *449*, No. 137682.

(20) Tao, B.; Ren, C.; Li, H.; Liu, B.; Jia, X.; Dong, X.; Zhang, S.; Chang, H. Thio-/LISICON and LGPS-type solid electrolytes for all-solid-state lithium-ion batteries. *Adv. Funct. Mater.* **2022**, *32*, 2203551.

(21) Yue, F.; Xia, Q.; Gong, Y.; Wang, M.; Xia, H.; Huang, X. A fully coupled electrochemical-mechanical-thermal model of all-solid-state thin-film Li-ion batteries. *J. Power Sources* **2022**, *539*, No. 231614.

(22) Zhou, B.; Bonakdarpour, A.; Stosevski, I.; Fang, B.; Wilkinson, D. P. Modification of Cu current collectors for lithium metal batteries- A review. *Prog. Mater. Sci.* **2022**, *130*, No. 100996.

(23) Saowadee, N.; Agersted, K.; Bowen, J. R. Lattice constant measurement form electron backscatter diffraction patterns. *J. Microsc.* **2017**, *266*, 200−210. https://www.x-mol.com/paperRedirect/1213024028956233728

(24) Chen, X.; Wang, Y.; Cao, G.; Zhang, T.; Gao, X.; Ming, H. Synergistic and capacitance effects in nanocarbon based capacitor batteries designed for superior rate capacity and long-cycle stability. *J. Colloid Interface Sci.* **2022**, *626*, 395−404.